Research Article

Syntheses, spectral characterization, single crystal X-ray diffraction and computational in gas and solid phases studies on *chloro- acetic acid N′-(2- hydroxy-naphthalen- 1-ylmethylene)- N-[4-(3-methyl-3-phenyl-cyclobutyl)-thiazol-2-yl]-hydrazide*

Tuncay Karakurt[1] · **Muharrem Dinçer**[2] · **Alaaddin Cukurovali**[3]

Received: 20 January 2020 / Accepted: 28 February 2020 / Published online: 7 March 2020

Abstract
In this study, the molecular structure of single crystal containing Schiff bases has been characterized by X-ray diffraction, NMR, IR and UV—Vis spectral techniques and compared with similar molecules in the literature. For the purpose of supporting X-ray results, geometric parameters and spectroscopic studies of the title compound were theoretically performed by Hartree—Fock and density functional theory methods. In addition, the title compound's molecular energies, Mulliken—ESP—NPA—Hirshfeld charges, molecular electrostatic potential surface, Frontier orbitals and thermodynamic properties to elucidate intermolecular interactions were calculated. All the calculations in gas and solid phases were carried out using Gaussian 09 and Quantum Espresso programs. It was found that the studies of X-ray are more compatible with the calculations made in the solid phase.

Keywords Schiff bases · X-ray · Quantum Espresso · DFT · Thermodynamic properties

1 Introduction

Aromatic heterocycle compounds have attracted more attention than poly ring cyclic aromatic compounds containing only carbon atoms, since they are very common in nature. Heterocyclic compounds also contain both carbon atoms and other atoms such as N, S and O in their structure. Thiazoles are also of the class of heterocycle compounds. In a ring of five, this compound is called thiazole if the sulfur and nitrogen atoms are in position 1 or 3. Many antibiotics and biomolecules containing thiazole and its derivatives are known to have biological importance. The compounds with thiazole ring have applications in pharmacology such as allergies [1], schizophrenia [2], hypertension [3], anti-HIV [4], anti-bacterial [5], anti-thrombotic activity [6], anti-protozoal [7], anti-helminthic [8], antimicrobial [9]. Furthermore, 2-aminothiazoles exhibit potential activity in many human cancer cell lines [10–13]. Thiazole rings are used as starting materials in many areas of chemistry. In addition, some thiazole compounds are used in the paint industry and in agriculture [14]. Cyclobutanes, which have a ring system with four carbon atoms, are organic compounds. There is bond tension in the cyclobutane ring, and because of this tension, the rings can easily react and be converted to straight-chain compounds. Furthermore, this tension makes the molecule more stable conformation by puckering the cyclobutane ring. Their carboxylic acid derivatives have antidepressant activity and liquid crystal properties. They are used

✉ Tuncay Karakurt, tuncaykarakurt@gmail.com | [1]Department of Chemical and Process Engineering, Faculty of Engineering-Architecture, Kırsehir Ahi Evran University, Kirsehir 40100, Turkey. [2]Department of Physics, Faculty of Arts and Sciences, Ondokuz Mayis University, Kurupelit, Samsun 55139, Turkey. [3]Department of Chemistry, Faculty of Science, Firat University, Elazig 23119, Turkey.

for different purposes, especially in the synthesis of heterocyclic substances [15].

In this paper, newly synthesized *chloro-acetic acid N'--(2-hydroxy-naphthalen-1-ylmethylene)-N-[4-(3-methyl-3-phenyl-cyclobutyl)-thiazol-2-yl]-hydrazide* was characterized with the help of X-ray diffraction, FT-IR, NMR and UV–VIS spectroscopy. Also, these spectroscopic studies, molecular energy, net charge, Molecular Electrostatic Potential (MEP) and boundary orbitals of the title compound were carried out theoretically.

2 Materials and methods

2.1 X-ray crystallography

Diffraction data of the head crystal were collected using the STOE IPDS II (Imaging Plate Diffraction System) diffractometer. X-AREA and X-RED32 [16] programs were used for data collection and reduction processes, respectively. After the necessary corrections had been applied to the collected data, the title compound was solved by direct methods with the help of SHELXT-2015 [17] software and refined by the least squares method with the help of SHELXL-2015 [18] software included in the Olex2 [19] packet program. All non–hydrogen atom parameters were refined anisotropically and all H atom parameters were located geometrically and refined by using a riding model with U_{iso} $(H) = xU_{eq}$, where x = 1.5 for CH_3 and OH groups and 1.2 for CH_2 and CH groups. The U_{iso} values for H atoms are in the range 0.063–0.236.

2.2 Synthesis

The compound was synthesized as shown in Scheme 1 by the following procedure. To a stirred solution of 1-{[4-(3-methyl-3-mesityl-cyclobutyl)-thiazol-2-yl]-hydrazonomethyl}-naphthalen-2-ol (0.456 g, 1 mmol) in 30 mL of absolute ethanol, chloroacetyl chloride (1 mmol) in 10 mL of absolute ethanol was added dropwise in 2 h period at room temperature in the presence of 1 mmol triethylamine. After the mixture was stirred 2 h more and poured into water. Thus, precipitated solid substance was filtered off, washed with aqueous NH_3 solution several times and dried in air. Suitable single crystals for crystal structure determination were obtained by slow evaporation of its ethanol solution. Yield: 67%, melting point: 428 K. Characteristic IR bands: 3390 cm^{-1} ν(–OH), 2957–2858 cm^{-1} ν(aliphatics), 1706 cm^{-1} ν(C = O), 1623 cm^{-1} ν(C = N azomethine), 1593 cm^{-1} ν(C = N thiazole), 736 ν(C–Cl), 639 cm^{-1} ν(C–S–C thiazole). Characteristic ^{1}H NMR shifts ($CDCl_3$, δ, ppm): 1.60 (s, 3H, $-CH_3$ in cyclobutane), 2.18 (s, 6H, *o*–CH_3), 2.21 (s, 3H, *p*–CH_3), 2.66–2.70 (m, 4H, $-CH_2-$ in cyclobutane), 3.64 (q, *j* = 8.78 Hz, 1H, > C–H in cyclobutane), 4.62 (s, 2H, $-CH_2-Cl$), 6.70 (s, 2H, aromatics), 6.90 (d, *j* = 0.73 Hz, 1H, = CH-S), 7.24 (t, *j* = 6.22 Hz, 2H aromatics), 7.38–7.46 (m, 2H, aromatics), 7.80–7.88 (m, 2H, aromatics), 7.90 (d, *j* = 9.15 Hz, 1H, aromatics), 9.82 (s, 1H, azomethine), 11.51 (s, 1H, –OH D_2O exchangeable). Characteristic ^{13}C NMR shifts ($CDCl_3$, δ, ppm): 165.38, 160.15, 158.84, 157.05, 144.25, 135.44, 135.30, 134.88, 132.94, 130.57, 129.50, 128.57, 128.40, 124.21, 119.92, 119.23, 111.90, 107.61, 43.97, 42.79, 41.23, 31.71, 24.78, 21.65, 20.65.

2.3 Computational details

All theoretical calculations in the gas phase were performed by the Gaussian 09 program package [20] which use the density functional theory (DFT)/B3LYP [21–23] functional and the 6–31G(d) [24] basis set. GaussView 5 [25] program was used to visualize the obtained results. The solid phase calculations were performed using the Quantum Espresso software [26] within the density functional theory (DFT). The correlation functionals were performed by the generalized gradient approximation (GGA), as proposed by Perdew–Burke–Ernzerhof (PBE) [27] and Local Density Approach (LDA), as proposed by Perdew-Zunger (PZ) [28].

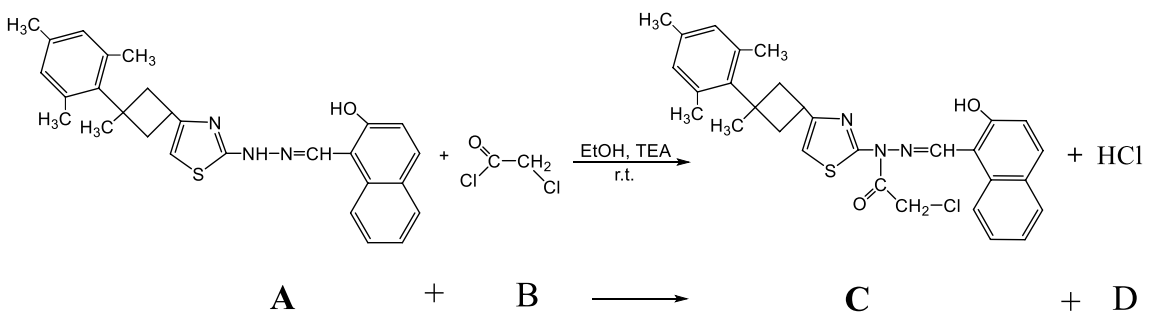

Scheme 1 Synthetic route for the synthesis of the target compound

3 Results and discussion

3.1 Geometrical structure

The crystal parameters, data collection and details of refinement process are shown in Table 1 and a diagram, which the crystal drawn with experimental 20% probability ellipsoids, is shown in Fig. 1.

The molecule has non-coplanar thiazole, cyclobutane, trimethyl benzene and naphthalene rings. The angles between the cyclobutane-thiazole and the cyclobutane-trimethyl benzene rings are 55.09° and 40.60°, respectively. Experimental and calculated bond lengths, bond angles and torsion angles are also shown in Table 3. The bond lengths of O1–C1, C11 = N1, C19–C17, S1 = C15, C22–C20 and C14 = N3 are experimentally 1.351 (3), 1.279 (3), 1.527 (4), 1.704 (2), 1.522 (4) and 1.303 (3) Å, respectively and these lengths are in accordance with the literature values [29, 30]. The crystal has C—H···O intermolecular and O—H···N and C—H···N intramolecular hydrogen bonds. The crystal is also stabilized by normal van der Waal's forces and by *π-π* stacking interactions between the naphthalene rings. The molecular structure has adopted the enol-imine form and has been stabilized by the O—H···N type intramolecular hydrogen bonding. The bond lengths C1—O1 showing the single bond character and C11 = N1 showing the double bond character support that the molecule adopts the enol-imine form. These bond lengths agree with the bond lengths obtained from similar enol-imine form structures [31, 32]. It is observed that C—H···O hydrogen bond between linking adjacent molecules formed a chain sequence along the b-axis direction with graph set analysis C(10) motif (Fig. 2) and N—H···O hydrogen bond generates an S(6) ring motif.

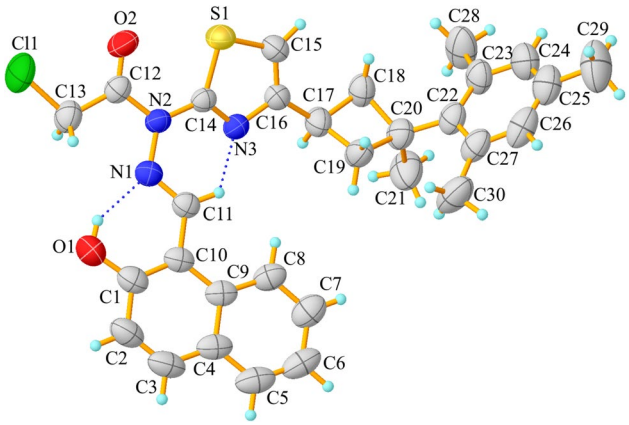

Fig. 1 ORTEP-3 shape of the title compound

Table 1 Data collection and refinement values of title compound

Empirical formula	$C_{30}H_{30}ClN_3O_2S$
Formula weight	532.08
Temperature/K	293 (2)
Crystal system	Monoclinic
Space group	$P2_1/c$
a/Å	16.4126 (9)
b/Å	23.5804 (9)
c/Å	7.1367 (4)
α/°	90
β/°	96.558 (4)
γ/°	90
Volume/Å^3	2743.9 (2)
Z	4
ρ_{calc}g/cm^3	1.288
μ/mm^{-1}	0.247
F (000)	1120.0
Crystal size/mm^3	0.50 × 0.28 × 0.14
Radiation	MoKα (λ = 0.71073)
2Θ range for data collection/°	2.498 to 53.574
Index ranges	− 20 ≤ h ≤ 20, − 29 ≤ k ≤ 29, − 9 ≤ l ≤ 8
Reflections collected	28,334
Independent reflections	5816 [R_{int} = 0.0683, R_{sigma} = 0.0514]
Data/restraints/parameters	5816/0/339
Goodness-of-fit on F^2	0.961
Final R indexes [I >=2σ (I)]	R_1 = 0.0505, wR_2 = 0.1088
Final R indexes [all data]	R_1 = 0.1000, wR_2 = 0.1257
Largest diff. peak/hole/e Å^{-3}	0.27/− 0.28
CCDC	761,391

In addition, within the title compound, there is a π···π interactions occur between the naphthalene rings of neighboring molecules linked by symmetry. The centroid–centroid distance between Cg1 (C4–C9) and Cg2^{ii} (C3/C4/C9/C1/C2/C10) [symmetry code: 1 − x, − 1/2 + y, 1/2 − z] is 3.959 (2) Å. As a result of the structure solution and refinement, ORTEP-3 of the obtained structure and the packaging drawing of the title compound in the unit cell are shown in Figs. 2 and 3, and the information about the hydrogen bindings are shown in Table 2.

In order that the stable molecular structure may be found, the global minimum scanning (2-dimensional PES analysis) were realized on the potential energy surfaces using AM1 semiempirical method [33]. Single point energies were calculated, which can affect the lowest energy conformation belonging to the molecule, changing the torsion angle θ (N1–N2–C14–S1) in steps of 10° ranging from − 180° to 180°. The two-dimensional single point energy profile versus the torsion angle is shown in Fig. 4. With the help of this graphic, global and local minimums were determined.

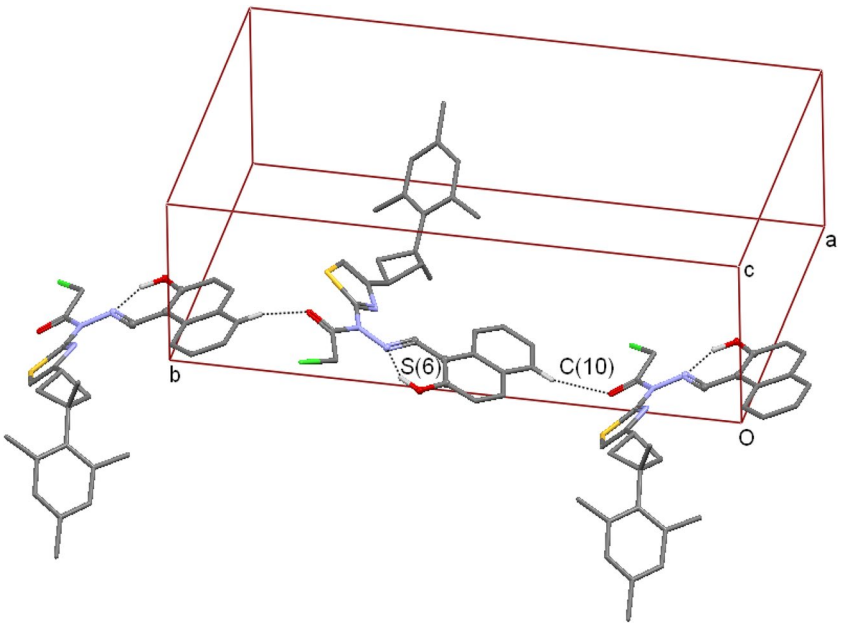

Fig. 2 Representation of intermolecular hydrogen bonds of the title compound. Hydrogens that do not contribute to binding have been deleted for clear indication

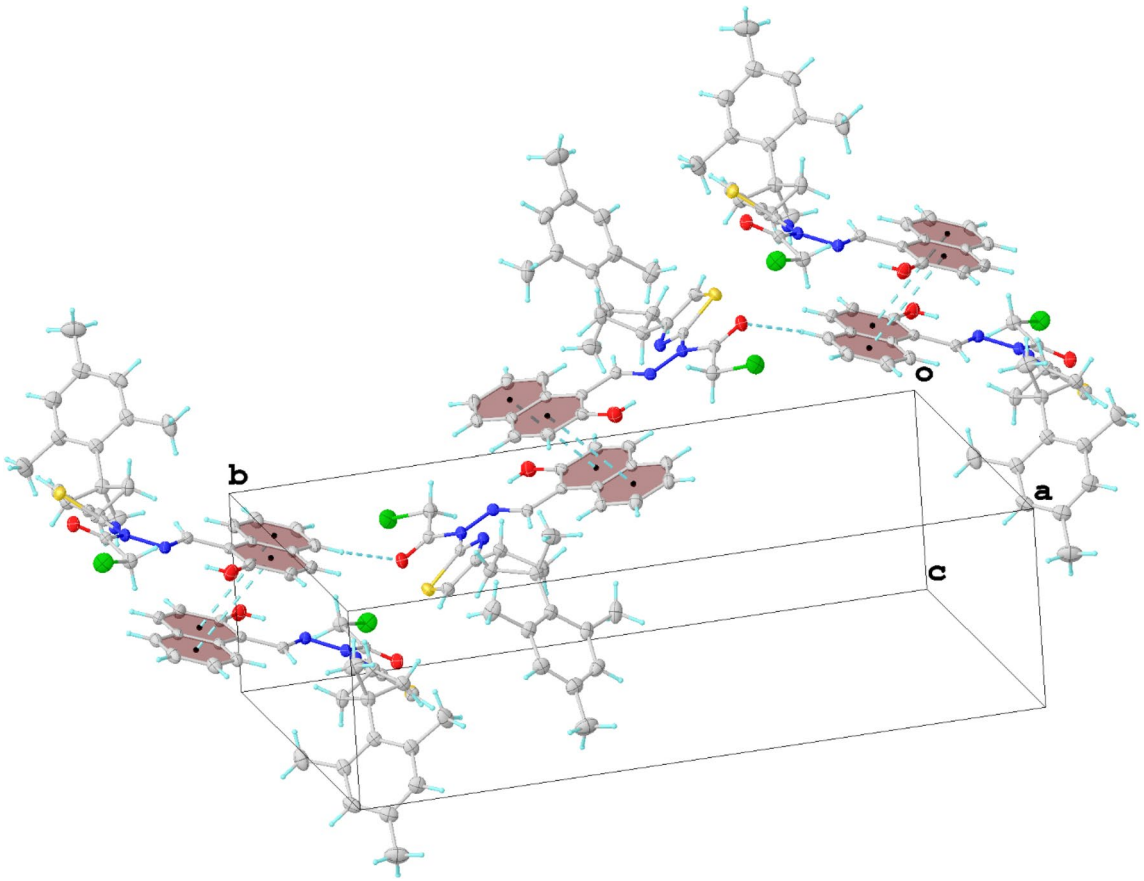

Fig. 3 Packing of the title compound with C—H···O and π—π interactions along the c axis

Table 2 Hydrogen bond geometry for the title single compound

D—H···A	D—H (Å)	H···A (Å)	D···A (Å)	D—H···A (°)
C5–H5···O2^{i}	0.930	2.130	2.767(3)	125
O1–H1···N1	0.820	1.930	2.643(3)	146
C11–11···N3	0.930	2.130	2.769(3)	125
Cg(I)	Cg(J)	Cg···Cg (Å)		
Cg1	Cg2^{ii}	3.959		

Symmetry codes (i): – x, + y– 1/2, – z + 1/2, (ii): – x, 1 – y, z

Cg1 the centroid of the (C4–C9) ring; *Cg2* the centroid of the (C3–C4/C9/C1–C2/C10) ring

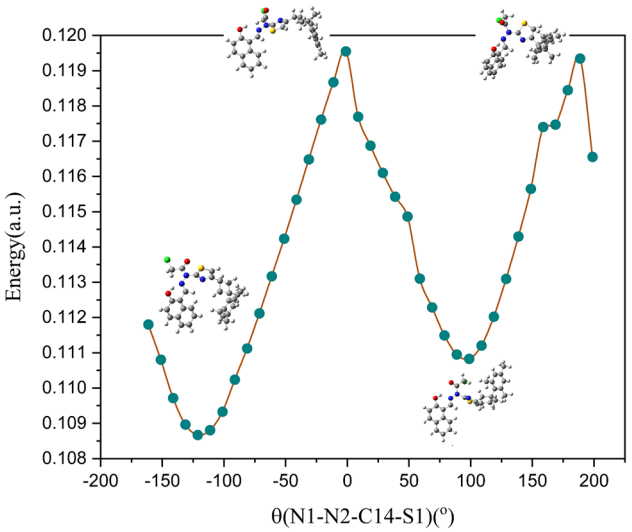

Fig. 4 Molecular energy profile versus the selected torsional degree of freedom

As seen in Fig. 4, the two most stable conformer (conf1 and conf2) were identified corresponding to global and local values at nearly – 120° and 100° angles. As a result of the re-optimization of the obtained two conformer, the corresponding total energy values were determined as – 2334.315800 a.u. (conf1) (Fig. 5a) and – 2334.310532 a.u. (conf2) (Fig. 5b). The conf1 conformation, which has a lower total energy, is more stable and has been used in all theoretical calculations.

Experimental and theoretical bond lengths, bond angles and torsional angles in the gas and solid phases of the title compound are listed comparatively in Table 3. When the calculated values in the Table 3 are examined, it is seen that HF method for bond lengths and B3LYP method for bond angles are more successful in representing experimental geometry in gas phase. Likewise, the GGA method has yielded better results than the LDA method for all parameters in the solid phase.

Figure 6 shows the overlap of X-ray and calculated molecular geometries. The RMS values resulting from the superposition of the experimental and theoretically structures were found to be 0.631 Å for HF level and 0.470 Å for B3LYP level. According to these results, DFT method has less error and characterizes the three dimensional structure of molecular geometry better than HF method.

3.2 Periodic boundary calculations (PBC)

The coordinates of 268 atoms in the unit cell were obtained from the cif file of the title compound and the kinetic energy cut-off (Ecut) value to model the system in the Plane Wave Self-Compliance field program was selected as 80 Ry. Furthermore, lattice constant was taken as 31.0155 a.u. and the numbers of k-point mesh for the Brillouin region were determined by MP (Monkhorst–Pack) method [34] and taken as 2 × 2 × 2. In order to increase the accuracy of the results of the total energy calculation, a convergence value of 10^{-6} Rydberg (Ry) was used. The optimized parameters of the unit cell were obtained using

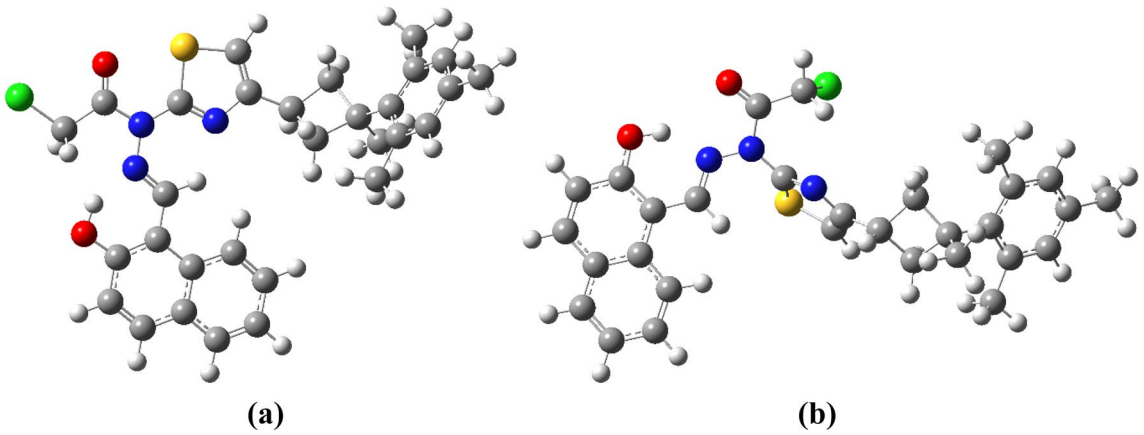

Fig. 5 Optimized conformations of the title compound crystal; **a** conf1, **b** conf2

Table 3 Some experimental and theoretically obtained geometric parameters

	X-ray	HF	DFT	LDA	GGA
Bond lengths (Å)					
O1–C1	1.351(3)	1.324	1.345	1.325	1.350
O2–C12	1.205(3)	1.189	1.215	1.219	1.226
N2–C14	1.406(3)	1.402	1.414	1.390	1.415
C14–N3	1.303(3)	1.275	1.304	1.302	1.311
C11–N1	1.279(3)	1.27	1.301	1.294	1.307
C12–N2	1.389(3)	1.379	1.404	1.377	1.403
S1–C15	1.704(2)	1.735	1.738	1.702	1.723
S1–C14	1.723(2)	1.739	1.768	1.721	1.752
N3–C16	1.379(3)	1.385	1.384	1.359	1.378
C17–C18	1.529(3)	1.535	1.543	1.537	1.553
C19–C17	1.527(4)	1.540	1.552	1.521	1.543
C20–C18	1.557(4)	1.563	1.574	1.554	1.575
C20–C21	1.544(4)	1.538	1.543	1.512	1.537
C22–C20	1.522(4)	1.536	1.534	1.504	1.530
RMS		0.010	0.012	0.015	0.012
Bond angles (°)					
C11–N1–N2	120.0(2)	124.93	123.27	120.08	120.81
N2–C12–C13	115.0(2)	114.27	115.71	115.20	115.46
O1–C1–C10	122.9(2)	124.35	122.58	121.26	121.41
C12–N2–N1	115.1(2)	116.94	114.03	116.38	115.18
C12–N2–C14	120.5(2)	122.36	119.73	119.11	119.36
N1–N2–C14	124.5(2)	122.85	126.22	124.49	125.44
C17–C18–C20	90.1(2)	89.67	89.74	89.705	90.51
C19–C17–C18	87.6(2)	88.01	88.01	88.400	88.40
C22–C20–C18	117.1(2)	117.98	118.14	116.84	116.14
C24–C23–C22	119.6(3)	120.09	119.87	119.74	119.75
C25–C24–C23	123.4(3)	122.37	122.50	122.32	122.66
RMS		1.896	1.346	0.860	0.841
Dihedral angles (°)					
N1–N2–C14–S1	− 161.16(15)	− 165.62	− 175.55	− 162.10	− 170.34
C12–N2–N1–C11	− 164.89(19)	129.60	178.40	− 167.94	− 162.99
C15–S1–C14–N3	− 0.4(2)	− 0.59	− 0.47	− 0.00	0.19
N3–C16–C17–C18	172.6(2)	− 171.81	− 171.54	174.23	179.78
C23–C22–C20–C19	− 143.46(18)	− 142.35	− 142.46	− 143.08	− 145.86
C23–C22–C20–C21	85.9(3)	89.40	88.32	88.00	85.04

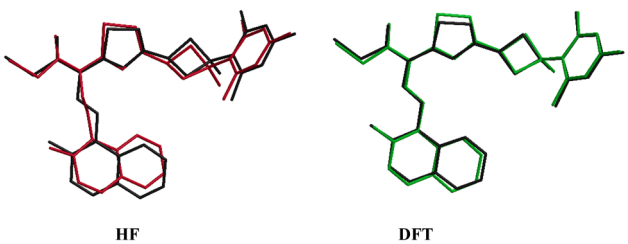

Fig. 6 The overlapping of the geometry (black) obtained from the X-ray diffraction of the crystal and the optimized geometries determined using HF and DFT methods

Table 4 Comparison of the experimental and optimized unit-cell parameters calculated by the Quantum ESPRESSO (QE) VC-Relax method

Unit cell parameters	Experimental X-ray	GGA PBE	LDA PZ
a (Å)	16.4126(9)	16.60550	15.79458
b (Å)	23.5804(9)	24.30976	22.88768
c (Å)	7.1367(4)	8.19235	6.70280
β (°)	96.558(4)	99.5814	96.5681°
Z	4	4	4
V (Å^3)	2743.9(2)	3260.9193	2407.1674

QE–VC-Relax method and BFGS (Broyden–Fletcher–Goldfarb–Shanno) quasi-Newton optimization algorithm. Table 4 shows the unit cell parameters obtained from X-ray and calculated using GGA and LDA methods while Fig. 7a–c is shown the distribution of atoms within the unit cell. In addition, the total lattice energy values per unit cell were obtained using the scf (*self-consistent field*) set included in Quantum-Espresso packet program for GGA and LDA methods. The energy values according to GGA and LDA methods were found to be − 2208.76400880 Ry and − 2201.94258365 Ry, respectively, which indicate that the GGA method has reached a more stable structure than the LDA method.

3.3 Spectroscopic studies

The experimental and calculated IR spectra of the title compound is shown in Fig. 8 and vibration frequency values are given in Table 5. The molecule has 195 normal modes of vibration. The essential characteristic vibrations of the title compound are C–H (aromatic), C = O, C = N (thiazole) and N–C = S vibrational frequencies connected to the ring groups were experimentally observed to be 3098, 1706, 1593 and 1207 cm^{-1}, respectively, as compatible with the literature [35, 36]. These modes have been calculated at 3083, 1781, 1476 and 1192 cm^{-1} for HF level and at 3148, 1726, 1472 and 1217 cm^{-1} for B3LYP level. While the O–H group, which does not contain an intramolecular or intermolecular hydrogen bonding, has a free vibration frequency between 3700 and 3550 cm^{-1}, this vibration frequency containing hydrogen bonding is observed between 3550 and 3200 cm^{-1} [37]. In our study, this frequency value was observed at 3293 cm^{-1}, while it

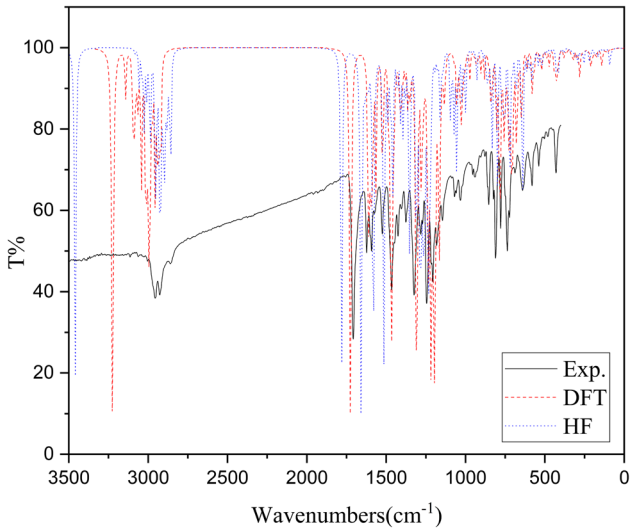

Fig. 8 Experimental and calculated IR spectra

was calculated at 3459 cm^{-1} for HF level and at 3224 cm^{-1} for B3LYP level and compares well with the value reported previously as 3436 cm^{-1} for experimentally and 3406 cm^{-1} for B3LYP level [38].

Experimental and calculated ^{1}H and ^{13}C chemical shift values for the title molecule are given comparatively in Table 6. The peaks of the C14, C15 and C 16 atoms in the ^{13}C-NMR spectrum (Fig. 9) may indicate that the molecule has a thiazole ring. The chemical shift values of these atoms are higher than other carbon atoms. Due to deshielding by the electronegative property of the N and S atoms, the chemical shift values of C14, C15 and C16 atoms are greater than the other carbon atoms and

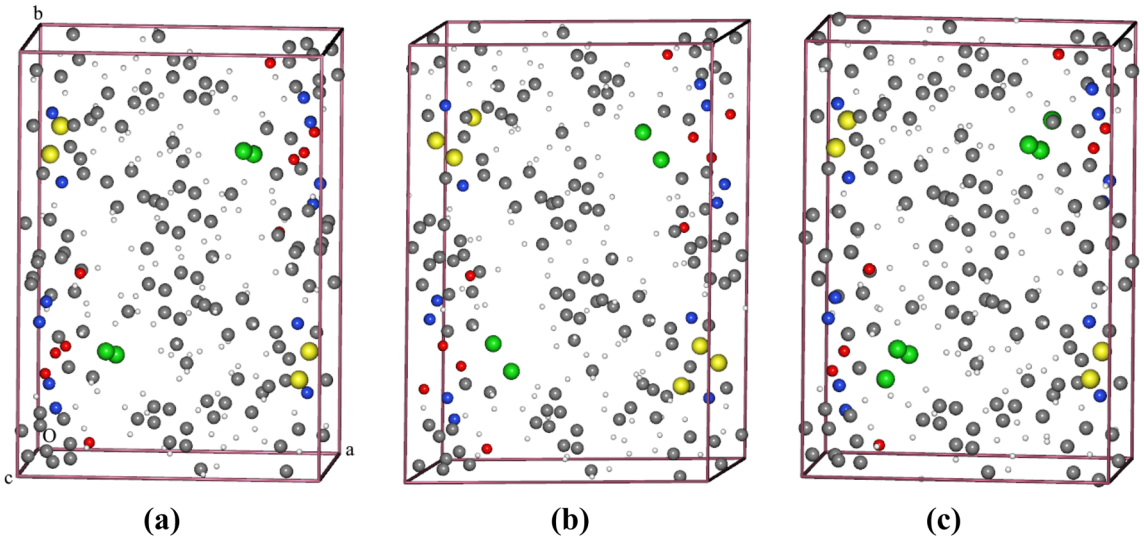

Fig. 7 Representation of atoms within the unit cell of the title compound **a** X-ray, **b** *QE–VC-relax*; GGA, **c** *QE-VC-Relax;* LDA

Table 5 Comparison of the experimental and calculated vibrational spectra

Assignments	FT-IR (cm^{-1})	Scaled frequencies (6–31G(d)) (cm^{-1})	
		HF	DFT
v O–H	3293	3459	3224
v ring C–H	3098	3083	3148
v aliphatic C–H	2957	3058	3141
v aliphatic C–H	2928	–	–
v C=O	1706	1781	1726
v azometine C=N	1623	1583	1565
v thiazole C=N	1593	1476	1472
v aromatic C–C	1572	1631	1602
v thiazole C=C	1525	1622	1599
ρ_s CH_2	1465	1573	1523
ρ_t aromatic C–H	1425	1466	1465
ρ_w CH_3	1376	1430	1426
v C–N	1324	1396	1386
ρ_t C–H + C–CH	1282	1287	1328
v C–N + ρ_w CH_2	1245	1230	1279
v N–C=S	1207	1192	1217
ρ_t aromatic C–H	1182	1179	1193
ρ_t aromatic C–H	1145	1142	1188
ρ_t N–H + ρ_t C–H + *v* C–N	1099	1132	1074
ρ_t C–H	1069	1074	1077
ρ_w CH_3	1032	1055	1034
ρ_w CH	954	973	947
v C–H	853	867	856
γ C–H	812	866	845
v C–Cl	778	799	784
γ C–H	736	756	731
γ C–H	638	641	647

v stretching; ρ_s makaslama; ρ_t rocking; ρ_w wagging; *γ* out of plane bending

were experimentally found to be 165.38, 107.61 and 153.3 ppm, respectively which is consistent with the values reported previously (168.54, 99.58 and 151.07 ppm) [38]. Similarly, the C1 and C12 carbon peaks linked to O1 and O2 atoms were experimentally found to be 157.05 and 160.15 ppm. These values agree with similar molecules [39]. The C1, C12, C14, C15 and C16 peaks were calculated at 162.95, 174.60, 173.11, 109.32 and 151.23 ppm for HF theory, respectively and at 153.3, 159.31, 155.56, 109.34 and 146.55 ppm for DFT theory.

In the ^{1}H-NMR spectrum (Fig. 10), the hydroxy hydrogen peak in the naphthalene ring was experimentally observed as a single proton peak at 11.51 ppm due to the formation of O–H•••N intramolecular hydrogen bonding.

Table 6 Experimental and calculated NMR spectra

Atoms	Experimental (ppm) ($CDCl_3$)	HF 6–31G(d) (ppm) ($CDCl_3$)	B3LYP 6–31G(d) (ppm) ($CDCl_3$)
C1	157.05	162.95	153.3
C2	119.23	114.58	112.13
C3	132.94	141.11	129.76
C4	130.57	124.27	121.22
C5	129.50	131.44	123.74
C6	119.92	121.02	117.09
C7	128.40	130.94	121.83
C8	124.21	117.94	114.1
C9	135.44	136.96	127.55
C10	111.90	101.41	104.2
C11	158.84	162.48	145.99
C12	160.15	174.60	159.31
C13	43.97	46.58	50.63
C14	165.38	173.11	155.56
C15	107.61	109.32	109.34
C16	153.3	151.23	146.55
C17	31.71	28.41	32.38
C18	42.79	35.56	39.84
C19	42.79	39.45	44.04
C20	24.78	35.64	44.09
C21	41.23	23.73	24.08
C22	144.25	142.62	138.1
C23	134.88	136.18	129.56
C24	128.57	128.67	124.09
C25	135.3	134.85	128.23
C26	128.57	128.57	124.05
C27	134.88	136.17	129.79
C28	20.65	21.56	22.57
C29	21.65	19.81	20.94
C30	20.65	21.34	22.78
H(OH)	11.51	10.85	10.04
H(CH_3 cyclobutane)	1.60	1.60–1.92	1.56–1.93
H(*o*–CH_3)	2.18	2.17–2.40	1.97–2.32
H (*p*–CH_3)	2.21	1.97–2.61	1.76–2.55
H (–CH_2 cyclobutane)	2.66–2.70	2.40–3.00	2.50–2.99
H (C–H cyclobutane)	3.64	3.59	3.86
H (–CH_2–Cl)	4.62	4.54–4.62	4.66–4.75
H (aromatic)	6.70–7.89	7.01–8.54	6.66–8.64
H(N=CH)	9.82	12.50	11.74
H(=CH-S)	6.90	5.43	6.28

In theoretical calculations, it was found that this peak was close to the experimental results at 10.85 ppm for HF and at 10.04 ppm for DFT.

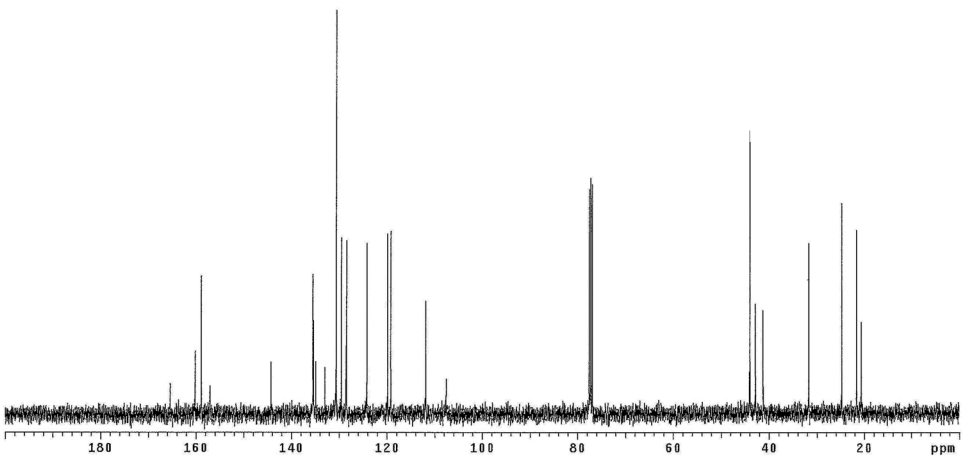

Fig. 9 ^{13}C NMR spectrum of target compound

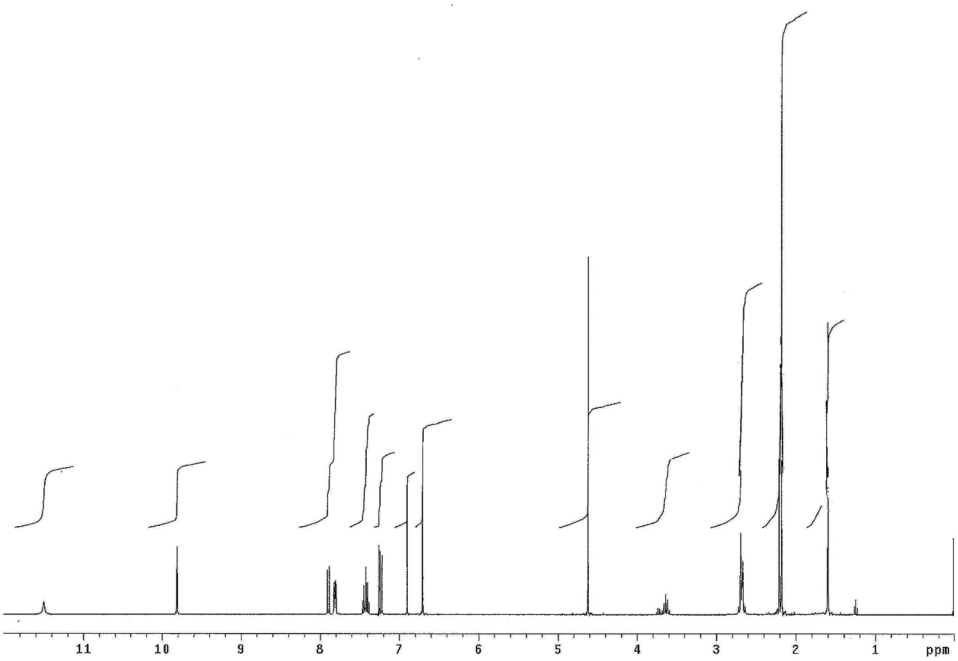

Fig. 10 ^{1}H NMR spectrum of target compound

3.4 Total charge distribution, electronic properties and MEPs of the title compound

Mulliken, ESP, NPA and Hirshfeld charge distributions of the title compound were calculated using the DFT/B3LYP/6–31G(d) method and are shown in Table 7. When the charge distributions are examined, it is seen that the most negative charges are collected on N, O and Cl atoms while the most positive charges are on C11, C12, C14, C16 and H1 (OH) atoms with neighboring electronegative atoms. Since these atoms are used in a strong intramolecular hydrogen bonding, the charge densities may be increased. As a result of theoretical calculations, the fact that both the N1 and N3 atoms are more negatively charged than the N2 atom and the O1 atom than the O2 atom support the intermolecular interactions within the crystal obtained by X-ray diffraction. According to these results, it is possible to say that these atoms play an important role in the formation of intermolecular hydrogen bonds.

Schiff bases obtained from aldehydes containing o-hydroxy group have two types of tautomeric structures: enol-imine and keto-amine. The presence of these two types structures was also determined by UV–VIS spectral analysis. It is known that electronic transitions occurring below 400 nm are enol-imine transitions and electronic transitions above 400 nm are keto-amine forms [40].

In our study, UV–VIS spectra (Fig. 11) of $C_{30}H_{30}N_3O_2SCl$ molecule were recorded in ethanol and it was determined that C = C, N–N and C = O groups may belong to

Table 7 Mulliken, ESP, NPA and Hirshfeld charges

Atoms	Mulliken	ESP	NPA	Hirshfeld
O1	− 0.543518	− 0.620822	− 0.67014	− 0.07609
O2	− 0.316729	− 0.476052	− 0.56762	− 0.2496
N1	− 0.376231	− 0.464844	− 0.38205	− 0.081197
N2	− 0.320716	− 0.076626	− 0.28657	0.001814
N3	− 0.3982	− 0.144398	− 0.55112	− 0.17071
S1	0.345211	0.086626	0.44333	0.082128
Cl1	− 0.039878	− 0.109578	− 0.02771	− 0.08903
C1	0.283861	0.62824	0.39746	0.090429
C2	− 0.209474	− 0.308187	− 0.23809	0.005857
C3	− 0.192083	− 0.222032	− 0.12912	0.029339
C4	0.042201	0.108398	− 0.08012	− 0.015333
C5	− 0.211168	− 0.225695	− 0.16081	0.009711
C6	− 0.193433	− 0.149512	− 0.20627	− 0.001056
C7	− 0.198985	− 0.087315	− 0.17624	0.007563
C8	− 0.226593	− 0.337852	− 0.19679	− 0.002904
C9	0.001138	0.370369	− 0.0088	− 1.01E−4
C10	− 0.135345	− 0.684995	− 0.17873	− 0.049288
C11	0.037169	0.631222	0.11473	0.076351
C12	0.506353	0.718559	0.69702	0.177285
C13	− 0.63576	− 0.458508	− 0.43425	0.110769
C14	0.242139	0.144673	0.25162	0.104748
C15	− 0.489673	− 0.40026	− 0.41578	− 0.02537
C16	0.255446	0.082715	0.15582	0.024414
C17	− 0.288577	0.101774	− 0.22575	0.00405
C18	− 0.397613	− 0.426924	− 0.36538	0.013357
C19	− 0.38624	− 0.481257	− 0.35452	0.015278
C20	− 0.136972	1.102273	− 0.03828	0.007235
C21	− 0.596149	− 0.537262	− 0.55688	0.011724
C22	0.042416	− 0.799344	− 0.05055	− 0.017391
C23	0.092553	0.503086	− 0.00317	− 0.008579
C24	− 0.231652	− 0.584253	− 0.20522	− 0.021639
C25	0.07507	0.474382	− 0.01024	− 0.011029
C26	− 0.231643	− 0.569096	− 0.20464	− 0.020895
C27	0.09357	0.454103	− 0.00155	− 0.007661
C28	− 0.721792	− 0.453566	− 0.57494	0.021466
C29	− 0.678798	− 0.433329	− 0.5703	0.030066
C30	− 0.722128	− 0.388889	− 0.57546	0.023827
H1	0.429121	0.391567	0.49022	0.137013
H11	0.312528	− 0.150880	0.22710	0.047622

$\pi \rightarrow \pi^*$ and $n \rightarrow \pi^*$ transitions. The two major maximum peaks observed in the experimental UV–VIS spectra are at 306.57 nm (molar absorption coefficient; $\varepsilon = 2800$ L/mol cm) and 277.24 nm (molar absorption coefficient; $\varepsilon = 3050$ L/mol cm). These values correspond to the transitions $n \rightarrow \pi^*$ and $\pi \rightarrow \pi^*$, respectively. This result supports that the molecule crystallizes in enol-imine form and agree with similar molecule [41]. Using the DFT method, these peaks were theoretically obtained

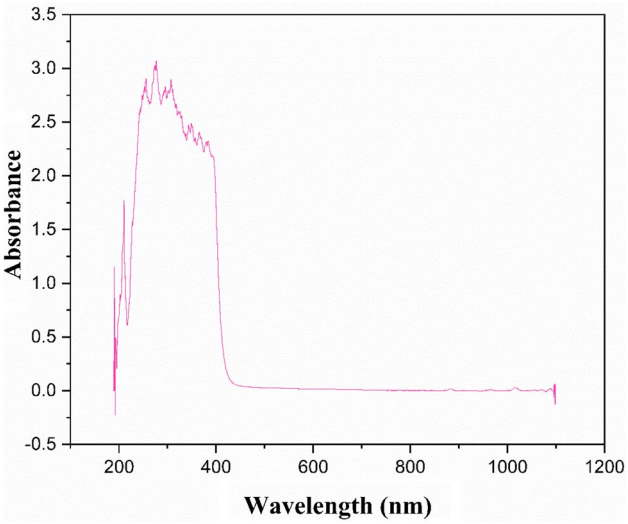

Fig. 11 Experimental UV–Vis spectrum

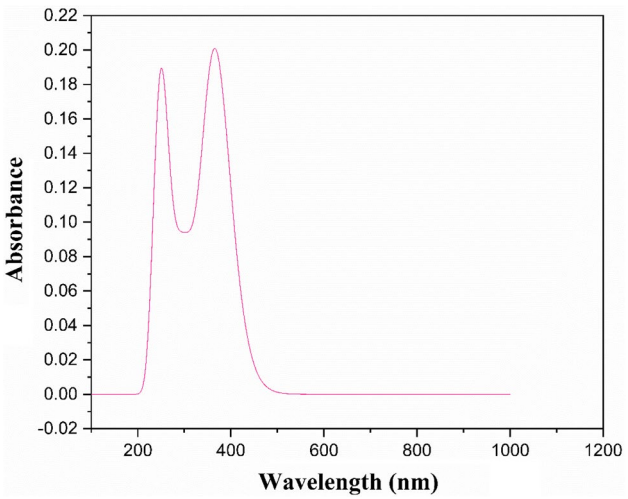

Fig. 12 Theoretically UV–Vis spectrum

at 366.93 nm ($\varepsilon = 20{,}089$ L/mol cm) and 249.13 nm ($\varepsilon = 18{,}833$ L/mol cm) (Fig. 12) and the two peaks correspond to the electron transitions HOMO → LUMO (98%) for 366.93 nm and HOMO-6 → LUMO (9%), HOMO-5 → LUMO (60%), HOMO-4 → LUMO (2%), HOMO-4 → LUMO + 2 (3%), HOMO-3 → LUMO + 1 (2%), HOMO-3 → LUMO + 2 (4%), HOMO → LUMO + 3 (16%) for 249.13 nm. The experimental and calculated two major maximum peaks of UV–Vis spectral data (excitation energies, wavelength, oscillator strength) were showed comparatively in Table 8.

The HOMO and LUMO orbitals and energy values of the title compound are given in Fig. 13. As it is seen, the orbitals, which the molecule react by giving electron,

Table 8 Experimental and calculated absorption wavelength (λmax), excitation energies (E), Oscillator strength (f), assignment and Excited State of the title compound

Major excited state and contributions	E (eV)	Wavelength (nm)		Oscillator strength (f)	Assignment
		Experimental	Calculated		
Excited state-1					
H → L (%98)	3.379	306.57	366.93	0.4850	n → π*
Excited state-2					
H-6 → L (%9)	4.977	277.24	249.13	0.2570	π → π*
H-5 → L (%60)					
H-4 → L (%2)					
H-4 → L+2 (%3)					
H-3 → L+1 (%2)					
H-3 → L+2 (%4)					
H → L+3 (%16)					

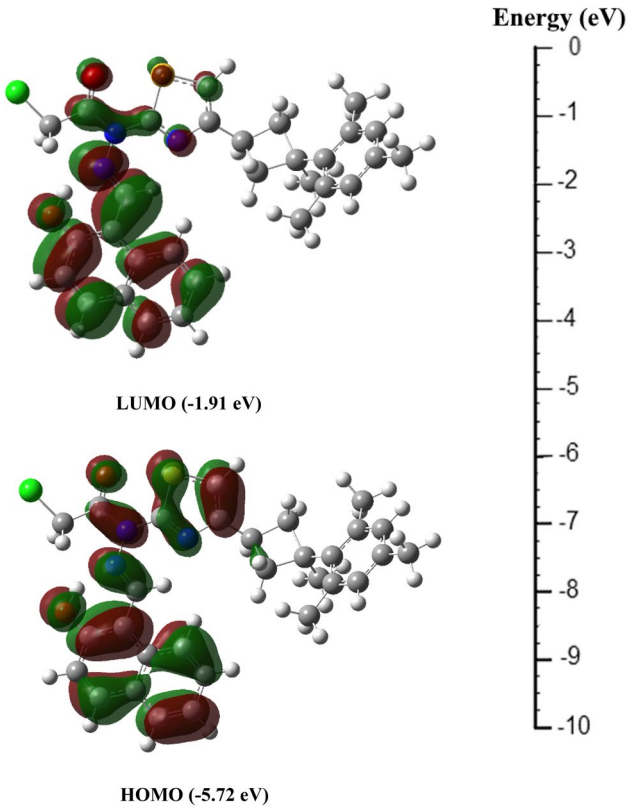

Fig. 13 HOMO and LUMO orbitals

are located on thiazole and naphthalene rings and the orbitals, which the molecule react by taking electron, are located on naphthalene, thiazole rings and N atoms. These orbitals on the compound indicate the regions where nucleophilic and electrophilic attacks occur.

The MEP map of the molecule was obtained using the DFT/B3LYP/6–31G(d) method and is shown in Fig. 14a, b. In the MEP map, negative regions (red, yellow) are on O and S atoms, while positive regions (blue) are on hydrogen atoms. The most negative region is on O atoms and the maximum MEP value is − 0.050 a.b., while the MEP value for S atom is − 0.035 a.b. and these results indicate that O and S atoms are the most suitable regions for electrophilic reaction. The maximum MEP value in the positive region on the H atoms bound to the benzene and naphthalene rings was calculated as + 0.023 a.b.. According to these results, the nucleophilic and electrophilic regions determined by net charge analysis, Frontier orbitals (FMO) and MEP analysis are in good agreement with each other.

3.5 Thermodynamic parameters of the title compound

Scheme 1 shows the complete synthesis scheme of the title compound. Heat capacity (C_m^0), entropy (S_m^0) and enthalpy (H_m^0) values, which are the standard thermodynamic functions for each reagent and products in the formation reaction, were calculated and are listed in Table 9, while enthalpy change (ΔH), Gibbs free energy change (ΔG) and entropy change (ΔS) values were calculated and are listed in Table 10. As can be seen in Table 9, the standard heat capacity, entropy and enthalpy of reactance and products were calculated between 100 and 500 K temperature and it is seen that the (C_m^0), (S_m^0) and (H_m^0) values increase as the temperature increases. In Table 10, the ΔS values of the title compound are negative in all temperature and the ΔH values are positive. This result indicates that the formation of the title compound occurs between

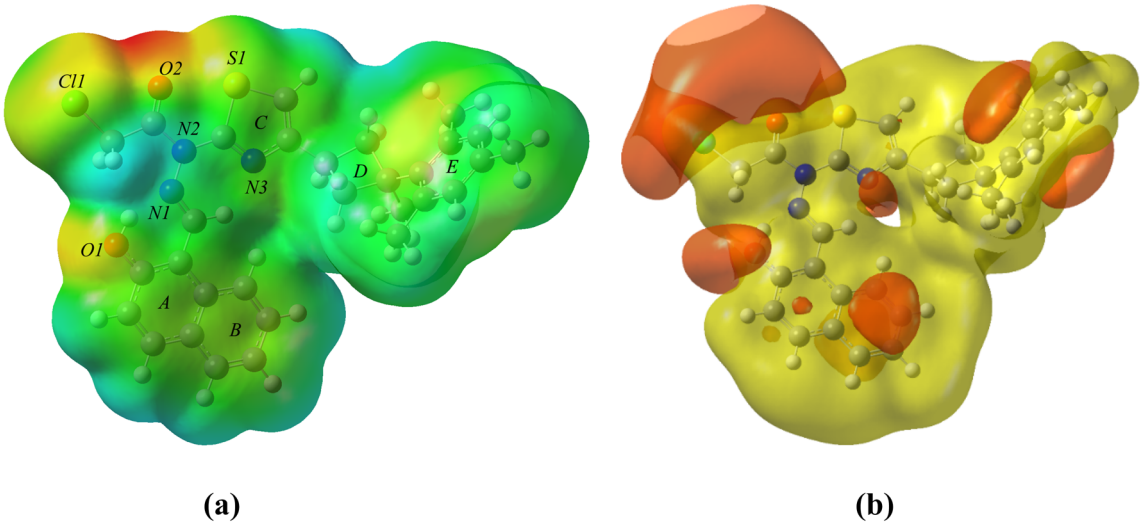

Fig. 14 **a** MEP map (blue arrow), **b** secondary MEP map derived from electron density

100 and 500 K by an endothermic process. Using the ΔG = ΔH − TΔS equation, Gibbs free energy change (ΔG) was also obtained between 100 and 500 K temperatures. In Table 10, the ΔG values above 100 K temperature are positive (ΔG > 0), indicating that the formation process of the title compound is not spontaneous.

According to the data in Table 9, The correlations equations of the C_m^0, S_m^0 and H_m^0 versus T temperatures were obtained as follows;

$$H_m^0 = -2.040884 + 0.083518\mathrm{T} + 7.321438 \times 10^{-4},\ \mathrm{T}^2\left(\mathrm{R}^2 = 0.999984\right)$$

$$C_m^0 = 50.983585 + 1.649169\mathrm{T} - 3095901 \times 10^{-4},\ \mathrm{T}^2\left(\mathrm{R}^2 = 0.999749\right)$$

$$S_m^0 = 311.759639 + 2.134661\mathrm{T} - 5.93033 \times 10^{-4},\ \mathrm{T}^2\left(\mathrm{R}^2 = 0.999887\right)$$

The values C_m^0, S_m^0 ve H_m^0 can be obtained at all other temperatures with these equations. Also, their correlation graphs are shown in Fig. 15.

The sign and size of these thermodynamic parameters are useful for determining the intermolecular binding mode (particularly receptor-ligand interactions). It has been reported that a hydrophobic interaction is characterized by ΔH > 0 and ΔS > 0 and van der Waals force or hydrogen bond formation is characterized by ΔH < 0 and ΔS < 0. However, ΔH ≃ 0 and ΔS > 0 are caused by an electrostatic force [42]. In our study, negative values of calculated ΔH and ΔS at temperatures corresponding to 100–500 K range indicate that van der Waals force or hydrogen bond interactions may play an important role in binding the title compound to a receptor. In addition, negative values of ΔG indicate the nature of the spontaneous formation of the binding process [43].

4 Conclusions

In this study, molecular structure of *chloro-acetic acid N'--(2-hydroxy-naphthalen-1-ylmethylene)-N-[4-(3-methyl-3-phenyl-cyclobutyl)-thiazol-2-yl]-hydrazide* crystal has been determined by X-ray diffraction and IR, NMR and UV–Vis spectroscopic methods. In addition, spectroscopic spectra were obtained theoretically. Finally, the Mulliken, ESP, NPA and Hirshfeld charge distributions, molecular electrostatic potential and FMO were investigated. The geometric

Table 9 Thermodynamic properties of the reactants and products at various temperatures

Structure	Temperature (K)	H_m^0 (kJ/mol)	C_m^0 (J/molK)	S_m^0 (J/molK)
Reactants				
A	100	11.82218756	196.196128	469.9477779
	150	23.50811085	273.006	563.7145103
	200	38.84793544	348.92468	651.4883447
	250	57.86437204	426.111112	736.0686482
	298.5	79.70198381	500.954504	815.7782137
	350	107.0557753	579.747592	900.2257886
	400	137.0641968	651.716576	980.2772309
	450	170.4085695	718.342592	1058.764084
	500	206.8113183	779.098456	1135.432958
	ZPE	1289.003		
	E	− 4520436.958		
B	100	3.820446525	40.08272	246.0667834
	150	6.34890585	48.500928	266.4788353
	200	9.273540937	56.450528	283.2468835
	250	12.56911766	64.0152	297.9274726
	298.5	16.07666104	70.87696	310.7418169
	350	20.19487024	77.69688	323.4676755
	400	24.47457784	83.654896	334.8903804
	450	29.02429058	89.002048	345.6051994
	500	33.81877433	93.780176	355.7046403
	ZPE	98.277		
	E	− 2816705.973		
Products				
C (title compound)	100	13.26810293	223.710112	501.440658
	150	26.48069078	308.712256	607.4867982
	200	43.71055132	391.835784	706.0920919
	250	64.95768458	476.022048	800.5988868
	298.5	89.25814695	557.379928	889.3018215
	350	119.5920886	642.792104	982.9478915
	400	152.7724396	720.61032	1071.469833
	450	189.5562236	792.51236	1158.04911
	500	229.6381077	857.966856	1242.472552
	ZPE	1364.799		
	E	− 6127579.111		
D	100	2.79594105	20.786112	148.8772616
	150	4.196434988	20.786112	160.2195249
	200	5.594405513	20.786112	168.2677054
	250	6.992376038	20.786112	174.5099723
	298.5	8.339878313	20.790296	179.4370193
	350	9.7908405	20.79448	183.9256597
	400	11.18881103	20.811216	187.6621713
	450	12.58930496	20.848872	190.9602763
	500	13.99232231	20.915816	193.9165045
	ZPE	16.847		
	E	− 1209588.697		

E total energies (kJ mol^{-1}); *ZPE* zero point energies (kJ mol^{-1})

Table 10 The entropy, enthalpy and free energy change of the formation reaction

Temperature	ΔH (kJ/mol)	ΔS (kJ/molK)	ΔG (kJ/mol)
100	− 30.089590	− 0.065696	− 23.519925
150	− 29.690891	− 0.062487	− 20.317837
200	− 29.327520	− 0.060375	− 17.252433
250	− 28.994429	− 0.058887	− 14.272613
298.5	− 28.691620	− 0.057781	− 11.472825
350	− 28.378716	− 0.056819	− 8.4917469
400	− 28.088524	− 0.056035	− 5.6742810
450	− 27.798332	− 0.055359	− 2.8863774
500	− 27.510663	− 0.054748	− 0.1363915

*$\Delta H = (H_m^0 + ZPE + E)_{productC} + (H_m^0 + ZPE + E)_{productD} - (H_m^0 + ZPE + E)_{reaktantA} - (H_m^0 + ZPE + E)_{reaktantB}$

*$\Delta S = (S_m^0)_{productC} + (S_m^0)_{productD} - (S_m^0)_{reaktantA} - (S_m^0)_{reaktantB}$

*$\Delta G = H_m^0 - T\Delta S$

parameters of the title compound in the gas and solid phases were calculated, and generally good agreement were observed when compared with the experimental structure. It was observed that the experimental and calculated IR values were consistent with the literature values. The presence of O–H and C = N stretching vibrations in the experimental IR spectrum supports that these molecules are in enol-imine form. When the charge distributions and molecular electrostatic potential surface were examined, it was observed that negative charges were generally located on electronegative atoms. The red and blue regions on the molecular electrostatic potential map represent regions that are prone to chemical reaction and are unstable to react.

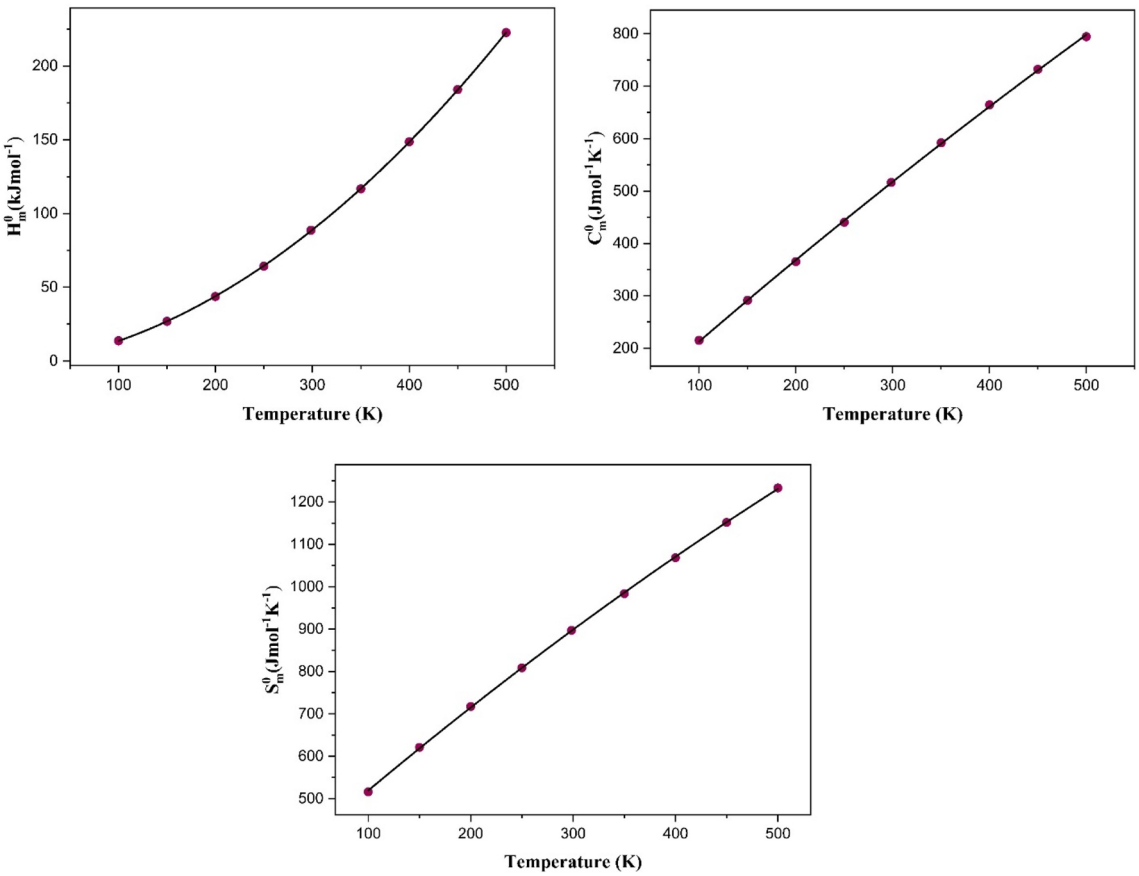

Fig. 15 Correlation graphs of the C_m^0, S_m^0 and H_m^0 versus various temperatures

Acknowledgements Computing resources used in this work were provided by the National Center for High Performance Computing of Turkey (UHeM) under Grant Number <5005172018>.

Compliance with ethical standards

Conflict of interest The author(s) declare that they have no competing interests.

References

1. Hargrave KD, Hess FK, Oliver JT (1983) *N*-(4-Substituted-thiazolyl) oxamic acid derivatives, new series of potent, orally active antiallergy agents. J Med Chem 26(8):1158–1163
2. Jaen JC, Wise LD, Caprathe BW, Tecle H, Bergmeier S, Humblet CC, Heffner TG, Meltzer LT, Pugsley TA (1990) 4-(1, 2, 5, 6-Tetrahydro-1-alkyl-3-pyridinyl)-2-thiazolamines: a novel class of compounds with central dopamine agonist properties. J Med Chem 33(1):311–317
3. Patt WC, Hamilton HW, Taylor MD, Ryan MJ, Taylor DG Jr, Connolly CJ, Doherty AM, Klutchko SR, Sircar I (1992) Structure-activity relationships of a series of 2-amino-4-thiazole-containing renin inhibitors. J Med Chem 35(14):2562–2572
4. Bell FW, Cantrell AS, Hoegberg M, Jaskunas SR, Johansson NG, Jordan CL, Kinnick MD, Lind P, Morin JM Jr (1995) Phenethylthiazolethiourea (PETT) compounds, a new class of HIV-1 reverse transcriptase inhibitors. 1. Synthesis and basic structure-activity relationship studies of PETT analogs. J Med Chem 38(25):4929–4936
5. Tsuji K, Ishikawa H (1994) Synthesis and anti-pseudomonal activity of new 2-isocephems with a dihydroxypyridone moiety at C-7. Bioorg Med Chem Lett 4(13):1601–1606
6. Badorc A, Bordes M-F, de Cointet P, Savi P, Bernat A, Lalé A, Petitou M, Maffrand J-P, Herbert J-M (1997) New orally active non-peptide fibrinogen receptor (GpIIb-IIIa) antagonists: identification of ethyl 3-[*N*-[4-[4-[amino [(ethoxycarbonyl) imino] methyl] phenyl]-1, 3-thiazol-2-yl]-*N*-[1-[(ethoxycarbonyl) methyl] piperid-4-yl] amino] propionate (SR 121787) as a potent and long-acting antithrombotic agent. J Med Chem 40(21):3393–3401
7. Tapia RA, Prieto Y, Pautet F, Walchshofer N, Fillion H, Fenet B, Sarciron M-E (2003) Synthesis and antiprotozoal evaluation of benzothiazolopyrroloquinoxalinones, analogues of kuanoniamine A. Bioorg Med Chem 11(16):3407–3412
8. Srivastava S, Yadav R, Srivastava S (2004) Synthesis and biological activity of 4-oxothiazolidines and their 5-arylidenes. Indian J Chem 43B:399–405
9. Siddiqui HL, Zia-Ur-Rehman M, Ahmad N, Weaver GW, Lucas PD (2007) Synthesis and antibacterial activity of Bis [2-amino-4-phenyl-5-thiazolyl] Disulfides. Chem Pharmaceut Bull 55(7):1014–1017
10. Kayagil I, Demirayak S (2009) Synthesis and anticancer activities of some thiazole derivatives. Phosphorus Sulfur Silicon 184(9):2197–2207
11. Misra RN, Xiao H-y, Williams DK, Kim KS, Lu S, Keller KA, Mulheron JG, Batorsky R, Tokarski JS, Sack JS (2004) Synthesis and biological activity of *N*-aryl-2-aminothiazoles: potent pan inhibitors of cyclin-dependent kinases. Bioorg Med Chem Lett 14(11):2973–2977
12. El-Subbagh HI, Abadi AH, Lehmann J (1999) Synthesis and antitumor activity of ethyl 2-substituted-aminothiazole-4-carboxylate analogs. Archiv der Pharmazie Int J Pharmaceut Med Chem 332(4):137–142
13. Gorczynski MJ, Leal RM, Mooberry SL, Bushweller JH, Brown ML (2004) Synthesis and evaluation of substituted 4-aryloxy- and 4-arylsulfanyl-phenyl-2-aminothiazoles as inhibitors of human breast cancer cell proliferation. Bioorg Med Chem 12(5):1029–1036
14. Schrauzer GN, Kohnle J (1964) Coenzym B12-modelle. Chem Ber 97(11):3056–3064
15. Çukurovali A, Taş E, Ahmedzade M (1997) The synthesis and some transition metal complexes of tolyl n-imidazolylmethyl ketoxime. Synth React Inorg Metal Chem Org 27(8):1115–1166
16. Cie S (2002) X-area (version 1.18) and X-red32 (version 1.04). Darmstadt, Germany
17. Sheldrick GM (2015) SHELXT–integrated space-group and crystal-structure determination. Acta Crystallogr Sect A Found Adv 71(1):3–8
18. Sheldrick GM (2015) Crystal structure refinement with SHELXL. Acta Crystallogr Sect C Struct Chem 71(1):3–8
19. Dolomanov OV, Bourhis LJ, Gildea RJ, Howard JA, Puschmann H (2009) OLEX2: a complete structure solution, refinement and analysis program. J Appl Crystallogr 42(2):339–341
20. Frisch M, Trucks G, Schlegel HB, Scuseria G, Robb M, Cheeseman J, Scalmani G, Barone V, Mennucci B, Petersson G (2009) Gaussian 09, revision A. 02, Gaussian. Inc., Wallingford, CT 200
21. Hohenberg P, Kohn W (1964) Inhomogeneous electron gas. Phys Rev 136(3B):B864
22. Lee C, Yang W, Parr RG (1988) Development of the Colle-Salvetti correlation-energy formula into a functional of the electron density. Phys Rev B 37(2):785
23. Becke AD (1993) Density-functional thermochemistry. III. The role of exact exchange. J Chem Phys 98(7):5648–5652
24. Foresman JB, Frisch A (1996) Exploring chemistry with electronic structure methods, 2nd edn. Gaussian Inc., Pittsburg
25. Dennington R, Keith T, Millam J, Eppinnett K, Hovell WL, Gilliland R (2009) GaussView, Version
26. Giannozzi P, Baroni S, Bonini N, Calandra M, Car R, Cavazzoni C, Ceresoli D, Chiarotti GL, Cococcioni M, Dabo I (2009) QUANTUM ESPRESSO: a modular and open-source software project for quantum simulations of materials. J Phys Condens Matt 21(39):395502
27. Perdew JP, Burke K, Ernzerhof M (1996) Generalized gradient approximation made simple. Phys Rev Lett 77(18):3865
28. Perdew JP, Zunger A (1981) Self-interaction correction to density-functional approximations for many-electron systems. Phys Rev B 23(10):5048
29. Sun Y-X (2006) 4-(5-Chloro-2-hydroxybenzylideneamino)-1, 5-dimethyl-2-phenyl-1H-pyrazol-3 (2H)-one. Acta Crystallogr Sect E Struct Rep Online 62(12):o5858–o5859
30. Sun Y-X, Zhang R, Jin Q-M, Zhi X-J, Lü X-M (2006) 4-(4-Chlorobenzylideneamino)-1, 5-dimethyl-2-phenyl-1H-pyrazol-3 (2H)-one and 4-(2-chlorobenzylideneamino)-1, 5-dimethyl-2-phenyl-1H-pyrazol-3 (2H)-one. Acta Crystallogr Sect C Cryst Struct Commun 62(8):o467–o469
31. Cukurovali A, Karakurt T (2019) Synthesis, spectroscopic, X-ray diffraction and tautomeric properties of 5-(diethylamino)-2-((2-(5-(3-methyl-3-phenylcyclobutyl)-6H-1, 3, 4-thiadiazin-2yl) hydrazono) methyl) phenol: a combined experimental and theoretical study. J Mol Struct 1189:328–337
32. Karakurt T, Cukurovali A, Subasi NT, Onaran A, Ece A, Eker S, Kani I (2018) Experimental and theoretical studies on tautomeric structures of a newly synthesized 2, 2′(hydrazine-1, 2-diylidenebis (propan-1-yl-1-ylidene)) diphenol. Chem Phys Lett 693:132–145
33. Dewar MJ, Zoebisch EG, Healy EF, Stewart JJ (1985) Development and use of quantum mechanical molecular models. 76. AM1: a new general purpose quantum mechanical molecular model. J Am Chem Soc 107(13):3902–3909

34. Monkhorst HJ, Pack JD (1976) Special points for Brillouin-zone integrations. Phys Rev B 13(12):5188
35. Rabie UM, Abou-El-Wafa MH, Nassar H (2012) Interaction of thiazolidine-2-thione with 2, 3, 5, 6-tetrabromo-1, 4-benzoquinone: a set of sequential interactions involving redox and substitution reactions after an initial charge transfer complexation. Spectrochim Acta Part A Mol Biomol Spectrosc 86:252–255
36. Lambert JB, Shurvell HF, Lightner DA, Cooks RG (1987) Introduction to organic spectroscopy. Macmillan Publishing Company, New York
37. Dabbagh HA, Teimouri A, Chermahini AN, Shahraki M (2008) DFT and ab initio study of structure of dyes derived from 2-hydroxy and 2,4-dihydroxy benzoic acids Spectrochim. Acta Part A Mol Biomol Spectrosc 69:449
38. Karakurt T, Cukurovali A, Subasi NT, Kani I (2016) Molecular structure and computational studies on 2-((2-(4-(3-(2, 5-dimethylphenyl)-3-methylcyclobutyl) thiazol-2-yl) hydrazono) methyl) phenol monomer and dimer by DFT calculations. J Mol Struct 1125:433–442
39. Yilmaz I, Çukurovali A (2003) Salicylaldehyde thiazolyl hydrazones as ligands. Heteroat Chem Int J Main Group Elem 14(7):617–621
40. Ünver H (2001) Synthesis and spectroscopic studies in some new Schiff bases. Spectr Lett 34(6):783–791
41. Joshi H, Kamounah FS, Gooijer C, van der Zwan G, Antonov L (2002) Excited state intramolecular proton transfer in some tautomeric azo dyes and schiff bases containing an intramolecular hydrogen bond. J Photochem Photobiol A Chem 152(1–3):183–191
42. Ross PD, Subramanian S (1981) Thermodynamics of protein association reactions: forces contributing to stability. Biochemistry 20(11):3096–3102
43. Mohamadi M, Faghih-Mirzaei E, Ebrahimipour SY, Sheikhshoaie I, Haase W, Foro S (2017) Synthesis, spectroscopic studies, DFT calculations, electrochemical evaluation, BSA binding and molecular docking of an aroylhydrazone-based cis-dioxido Mo (VI) complex. J Mol Struct 1139:418–429